NJC

New Journal of Chemistry

A journal for new directions in chemistry

Accepted Manuscript

Volume 42
Number 6
21 March 2018
Pages 3963-4776

NJC

New Journal of Chemistry

A journal for new directions in chemistry

rsc.li/njc

ISSN 1144-2546

PAPER
Chechia Hu, Tzu-Jen Lin *et al*
Yellowish and blue luminescent graphene oxide quantum dots prepared via a microwave-assisted hydrothermal route using H2O2 and KMnO4 as oxidizing agents

ROYAL SOCIETY OF CHEMISTRY

CNRS

ROYAL SOCIETY OF CHEMISTRY

rsc.li/njc

ARTICLE

Ammonium monoethyloxalate (AmEtOx): a new agent for the conservation of carbonate stone substrates

M. Carla Aragoni,[a] Laura Giacopetti,[a] Massimiliano Arca,[*a] Gianfranco Carcangiu,[b] Stefano Columbu,[a] Domingo Gimeno,[e] Francesco Isaia,[a] Vito Lippolis,[a] Paola Meloni,[c,d] Antonia Navarro Ezquerra,[f] Enrico Podda,[a] Jordi Rius,[g] Oriol Vallcorba,[h] and Anna Pintus[*a]

The ammonium salt of monoethyloxalate (AmEtOx) was investigated as a novel precursor for the conservation of carbonate stone substrates, such as biomicritic limestone and marble. A full characterization of treated and untreated authentic stone samples was carried out by means of SEM microscopy, X-ray powder diffraction, synchrotron tts-μXRD measurements, mercury intrusion porosimetry, determination of water transport properties, and pull-off tests. The improved solubility (1.49 M, 20.1% w/w) of AmEtOx as compared to ammonium oxalate (AmOx; 0.4 M, 5% w/w) results in the formation of microcrystalline phases 30–50 and 200–500 μm thick of calcium oxalate mono- (whewellite) or dihydrate (weddellite) on marble and biomicrite samples, respectively, after the treatment with AmEtOx 5% and 12% w/w water solutions. As a result, a reduction in the porosity of the stone samples and an enhancement of their cohesion is observed. DFT calculations, carried out to investigate the hydrolysis reaction leading from AmEtOx to AmOx, showed that the localization of the Lowest Unoccupied Molecular Orbital (LUMO) and the natural charge distribution account nicely for the tendency to hydrolysis observed experimentally, eventually leading to the formation of whewellite and weddellite on the stone surface.

[a] Università degli Studi di Cagliari, Dipartimento di Scienze Chimiche e Geologiche, S.S. 554 bivio per Sestu, 09042 Monserrato (Cagliari), Italy.

[b] Consiglio Nazionale Delle Ricerche (CNR), Istituto di Scienze dell'Atmosfera e Del Clima (ISAC), UOS di Cagliari c/o Dipartimento di Fisica, Università degli Studi di Cagliari, S.S. 554 bivio per Sestu, Monserrato (Cagliari), 09042, Italy

[c] Dipartimento di Ingegneria Meccanica, Chimica e dei Materiali, via Marengo 2, 09123, Cagliari, Italy

[d] Laboratorio Colle di Bonaria, Università degli Studi di Cagliari, Via Ravenna snc, Cagliari, 09125, Italy

[e] Facultat de Ciències de la Terra, Universitat de Barcelona, c/ Martí i Franquès s/n, 08028 Barcelona, Spain

[f] Departamento de Tecnología de la Arquitectura, EPSEB-UPC, Avda. Doctor Marañón, 44-50, 08028 Barcelona, Spain

[g] Institut de Ciència de Materials de Barcelona (CSIC), Campus de la UAB, 08193 Bellaterra, Spain

[h] ALBA Synchrotron Light Source − CELLS. 08290 Cerdanyola del Vallès, Barcelona, Spain

1. Introduction

Since antiquity, carbonate stones, such as limestone and marble, have been widely used as materials of buildings and sculptures. Unfortunately, carbonate natural stones and ancient mortars are vulnerable to various forms of weathering including physical, chemical, and biological phenomena.[1–9] The water solubility of calcite (K_{sp} = 3.27·10^{-9} at 25 °C)[10] is such that dissolution by rain (the so-called Karst effect) is one of the major causes of deterioration of marble and limestone artworks exposed outdoors.[11–14] Acid rains increase the dissolution rate of calcite and result in largely soluble byproducts, such as gypsum and calcium nitrate.[15–17] Moreover, due to its anisotropic thermal behaviour, particularly in the linear and cubic thermal expansion coefficients, calcite can undergo decay induced by day/night temperature variations and heating/cooling cycles. These stresses lead to displacement of calcite grains, detachment of grain boundaries, and onset of triple points of stress concentrator. The stone undergoes weakening and a microcracks network develops.[18–20] These weathering phenomena result in the so-called marble "sugaring" (i.e. grain detachment and loss)[21] at the micro-scale, and bowing of marble slabs at the macro-scale, especially in the presence of structural constraints.[15] Even when the loss of material is limited to the surface and negligible to the structural stability of the affected artifacts, it can represent a major problem in carved decorative stone elements of artistic value, where any details should be preserved,[22] as well as the ancient carbonate-based mortars used for their laying.[23,24] Porous calcareous materials, on the other hand, are susceptible to the crystallization of salts into confined pores, the resulting pressure leading to spalling and cracking of the material.[25] In order to reduce the effects of weathering processes, restoring and consolidating chemicals can be applied as either solutions or colloidal suspensions, able to penetrate the stone void network where a solid phase can precipitate or polymerize,[26] thus partially restoring the cohesion between stone grains and reducing the rate of rock decay and the loss of material.[27] Consolidation treatments need to comply with compatibility and durability requirements,[3] as well as with other general conservation ethics, and as a consequence, choosing a proper consolidant is a

challenging task.[28] Since the 19th century, craftsmen and restorers have been applying a variety of natural and synthetic products to stone elements with the aim of regaining strength and cohesion. The traditional consolidating Ca(OH)$_2$ product is typically applied as a saturated water solution (limewater) and the consolidating action is due to the spontaneous conversion to CaCO$_3$ by atmospheric CO$_2$.[29,30] Its main limitations are the very low solubility in water and the scarce penetration depth, which do not result in a satisfactory strengthening effect.[31,32] During the past century, organic consolidants, such as acrylic and epoxy resins, have been extensively used in restoration treatments for carbonate stones due to their immediate strength enhancement, ease of application and the limitations shown by limewater.[33] However, they lack chromatic and physical compatibility with the substrate[34] and tend to undergo photo-oxidative decay processes promoted by the direct action of sunlight in outdoors environments.[35,36] In this context, a promising approach was the use of fluorinated oligomeric compounds or polymers.[37] Hydrophobic fluorinated oligoamides[38] and acrylic polymers,[39] for instance, have been successfully tested on the laboratory scale. This notwithstanding, synthetic organic polymers have been considered not suitable for the preservation of ancient stone artifacts,[40] and research has recently mainly focused on inorganic consolidants.[41] Alkoxysilane-based formulations, such as those based on methyltrimethoxysilane (MTMOS), have been the most widely used consolidants over the past twenty years, and in particular tetraethoxysilane (TEOS) based products are still largely used. These compounds penetrate into stone pores, undergo hydrolysis by reacting with water, and the subsequent condensation provides silica gel.[42] Although good results were obtained on siliceous stones, a similar result cannot be achieved when they are applied to carbonate stones, unless they contain large silicate fractions.[43] Treatments based on the consolidating effect of diammonium hydrogen phosphate (NH$_4$)$_2$(HPO$_4$) (DAP),[16,44–50] and the passivating/protective action of ammonium oxalate (NH$_4$)$_2$(C$_2$O$_4$) (AmOx),[3,51–54] have been proposed over the past two decades. When in contact with a carbonate substrate, DAP reacts with the calcium ions to form hydroxyapatite (HAP), while the application of AmOx (or in some cases oxalic acid)[55] on the surface of

Journal Name

ARTICLE

carbonate stones generates whewellite (calcium oxalate monohydrate $CaC_2O_4 \cdot H_2O$, $K_{sp} = 2.0 \cdot 10^{-9}$ at 25 °C),[56,57] and/or metastable weddellite (calcium oxalate dihydrate, $CaC_2O_4 \cdot 2H_2O$, $K_{sp} = 3.8 \cdot 10^{-9}$ at 25 °C),[58–61] which are also naturally formed on stone:[62,63]

$$CaCO_{3(s)} + (NH_4)_2(C_2O_4)_{(aq)} \rightarrow Ca(C_2O_4) \cdot H_2O + 2\ NH_{3(g)} + CO_{2(g)}$$
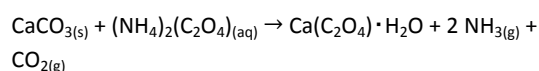
The lowest solubility of whewellite as compared to calcite and its stability under acidic pH result in an increased chemical resistance and effective consolidating and protecting capabilities. However, AmOx does not react sufficiently in depth into the stone (Table S1 in ESI).[64–68]

Over the past few years, the efforts of researchers have mostly been focused on improving the application procedures of the aforementioned products,[69–73] also by the use of nanoparticles.[74–81] Bioremediation techniques employing bacterial species or fungi for the biomineralization of calcium carbonate[82–87] or, more rarely, calcium oxalate[88,89] on different carbonate substrates were also explored, providing encouraging preliminary results, but needing further studies concerning the geographical and environmental variabilities of the process, as well as the risks posed by aesthetic and mineral changes induced by biomineralization.[90–93]

Few efforts have been made to synthesize new materials related to the most used inorganic consolidants in order to overcome their shortcomings. Recently, some of the authors have started to explore this approach through the functionalization of one of the two carboxylate groups of AmOx, in order to synthesize salts of new monoester or monoamide (oxamates) derivatives with greater solubility, while possibly decreasing the solubility of the correspondent calcium salts. In particular, the ammonium salts of monomethyloxalate (AmMeOx), oxamate (AmOxam),[94] and phenyloxamate (AmPhOxam)[95] were successfully tested as conservation agents for white Carrara marble and biomicritic limestone, and a computational investigation on the interaction of these systems with calcite was recently reported.[96] Notwithstanding these promising results, we have been continuously testing differently monosubstituted oxalate and oxamate inorganic derivatives in the search of a more soluble alternative to the previously tested salts (AmMeOx,

AmOxam, and AmPhOxam). In this paper, we report on the synthesis and characterization of ammonium monoethyloxalate AmEtOx, proposed as a conservation agent of carbonate stone substrates. In addition to the study of the petrographic-compositional aspects of the stone substrate, some important physical (porosity, density, water absorption, capillarity, and ultrasonic velocity) and mechanical (pull-off tests) properties were compared before and after the treatments. In fact, the study of these parameters is strongly related to the minero-petrographic aspects and proves to be essential to define the decay processes of geomaterials used in the Cultural Heritage, and in the evaluation of the effectiveness of the consolidation and protection treatment adopted in the restore interventions.[97–100]

2. Experimental

2.1 Stone samples preparation and accelerated ageing procedure

A white marble variety ("Statuario Michelangelo") and a biomicritic limestone were supplied by Cava Carrarese (Carrara, Italy) and a disused mining site (Cava Flore) in Santa Caterina di Pittinuri (Oristano, Italy), respectively. Samples were obtained by slicing a piece of the same stone into a number of prism-shaped specimens with different size (1.0×0.4×0.4, 1.0×0.8×0.5, 4.0×4.0×0.5, 2.0×2.0×8.0, 3.0×3.0×3.0, or 2.0×2.0×2.0 cm). Lapped thin sections (with a thickness of about 30 µm) for transmitted polarized light microscopy (TPL) and tts-µXRD studies were obtained from the rock samples following the standard UNI 9724/4-90,[101] in order to perform the petrographic and mineralogical analyses, respectively.

Twenty prismatic (2.0×2.0×8.0 cm) Carrara marble samples were subjected to thermal treatment: the samples were positioned vertically in a Carbolite CWF 1200 muffle furnace, and the furnace temperature was ramped to 600 °C in 1 h, held at that temperature for 7 h and ramped down to 25 °C in 3 h. The samples were then subjected to a second thermal cycle under the same conditions, in order to confirm literature data indicating that similar properties can be observed after consecutive thermal treatments.[102] No artificial weathering treatment was performed on the biomicritic limestone samples, since the lack of

literature data on the environmental weathering of these lithotypes makes it difficult to directly compare microstructural modifications caused by heating with those induced by natural weathering.[102]

2.2 Synthesis and application of AmEtOx

A freshly prepared aqueous solution of NH_4HCO_3 (6.00 g, 759 mmol, 40 mL) was added to an aqueous solution of diethyl oxalate (9.90 g, 677 mmol, 40 mL). The resulting mixture was refluxed for 3 h, and subsequently evaporated at room temperature. The crude product was washed with diethyl ether. Yield 4.30 g (318 mmol, 47%); melting point 65 °C; FT-IR: $\tilde{\nu}$ = 3421 (m, broad), 3101 (s, broad), 2994 (m, broad), 1720 (vs), 1645 (vs), 1400 (s), 1205 (s), 1026 (w), 901 (vw), 781 (vw), 773 cm^{-1} (vw). UV–Vis–NIR (H_2O): l_{max} = 192 nm (e = 4590 M^{-1} cm^{-1}); elemental analysis calculated (%) for $C_4H_9NO_4$: C 35.55, H 6.71, N 10.37; found: C 35.19, H 6.31, N 10.85; ^{1}H-NMR (300 MHz, D_2O): d = 4.26 (q, 2H, –CH$_2$–), 1.32 (t, 3H, –CH$_3$) ppm.

Thermally treated stone samples of variable dimensions (see above) were immersed in freshly prepared 5% or 12% w/w aqueous solutions (50 mL) of AmEtOx (0.37 and 0.89 M, respectively) into a static batch for 24 h., i.e. under the same conditions adopted in our previous studies.[94,95] The pH of the solution was measured (pH = 4.2), and the samples were washed with water, dried at room temperature for 4 days, and then kept into a thermostatic heater (60 °C) for 24 h.

2.3 Materials and characterization techniques

Reagents and solvents were purchased from TCI and Sigma Aldrich and used without further purification. All tests for the physico-mechanical characterization of samples were run in triplicate. Elemental analyses were performed with a 2400 series II CHNS/O elemental analyzer (T = 925 °C). Melting points were recorded on a FALC melting point apparatus mod. C (up to 300 °C) and are uncorrected. FT-IR spectra were recorded by a Thermo-Nicolet 5700 spectrometer at room temperature: KBr pellets with a KBr beam-splitter and KBr windows (4000–400 cm^{-1}, resolution 4 cm^{-1}) were used. Absorption spectra were recorded at 25 °C in water in a quartz cell of 10.00 mm optical path by a Thermo Evolution 300 (190–600 nm) spectrophotometer. ^{1}H-NMR measurements were

carried out in D_2O at 25 °C, using a Bruker Advance 300 MHz (7.05 T) spectrometer at the operating frequency of 300.13 MHz. Chemical shifts are reported in ppm (d) and are calibrated to the solvent residue. Solubility and K_{sp} values at 25 °C were evaluated spectrophotometrically on saturated aqueous solutions, after recording a calibration curve on three samples.

Petrographic examinations (performed by following the European Standard UNI EN 12407:2007)[103] and optical observations of the stone samples were carried out using a Zeiss Axioskop 40 optical microscope with Zeiss camera Axiocam HR, operating in PPTL (plain polarized transmitted light) and CPL (cross polarized light) mode. Scanning Electron Microscopy (SEM) investigations were performed with a Zeiss Evo LS15 microscopy equipped with a LaB$_6$ filament as electron source. The pH of the solutions was determined with a Metrohm 691 pH meter. Ultrasonic pulse velocity (Vp) measurements were carried out before and after each thermal cycle on a CNS Electronics Pundit tester (precision ±0.1 ms). 150 MHz (1), 11.82 mm⌀ transducers were attached to the stone surface with Henkel Sichozell Kleister (carboxymethyl cellulose) paste to enhance the transducer-stone coupling. Ten Vp measurements were made directly and consecutively at different points along the three orthogonal axes and then averaged. The results were used to calculate the total (dM) and relative (dm) Vp anisotropy indices.[104–106]

Synchrotron through-the-substrate X-Ray microdiffraction (tts-μXRD)[107] measurements were performed at the microdiffraction/high-pressure station of the MSPD beamline (ALBA Synchrotron, Barcelona, Spain)[108] equipped with Kirkpatrick–Baez mirrors providing a monochromatic focused beam of 15 × 15 mm^2 (full width at half maximum) and a Rayonix SX165 CCD detector (round active area of 165 mm diameter, frame size 2048 × 2048 pixels, 79 mm pixel size, dynamic range 16 bit). The energy used was 29.2 keV (λ = 0.4246 Å), as determined from the Sn absorption K edge. The sample-to-detector distance and the beam center position were calibrated using the d2Dplot software[109] with LaB$_6$ as calibrant. The sample was mounted on a xyz stage with the thin section (~ 30 mm thickness) faced to the incoming beam and the measurement point selected with an on-axis ultrazoom microvisualization system (equipped with polarized

Journal Name

ARTICLE

light). The measurements were performed by rotating the sample ±5 ° around the vertical tilt axis. All patterns were taken under the same conditions. To remove most of the glass-substrate contribution (1.5 mm thickness), an additional 2D pattern of only the glass-substrate was collected. The final 'powder' diffraction pattern was obtained by circularly averaging the corresponding difference 2D pattern. In all measurements the illuminated area was the same.

Colorimetric measurements were carried out by using a Konica Minolta CM-700d spectrophotometer (illuminant D65). The instrument has been adjusted to repeat the measurement 6 times on each point: for each sample eight points have been identified and measured. The results were evaluated as L^* (brightness), a^* (redness colour), and b^* (yellowness colour) coordinates. The total colour difference ΔE was calculated according to the CIE-76 and CIE-2000 colour space standards.[110]

Mercury intrusion porosimetry (MIP) measurements were carried out on a Micromeritics Autopore IV 9500 up to 2200 bars. Stone skeletal densities were determined by a Micromeritics AccuPyc II 1340 He Pycnometer and introduced in the material parameter sheet of the software of the above-mentioned Porosimeter in order to calculate pore size distribution along with the apparent density. XRD-examination on powdered samples, aimed at investigating their mineralogical composition, was carried out on a Rigaku Miniflex II unit operating with Cu tube at 30 kV and 15 mA. The mineralogical phases were determined by comparison with ICDD (International Centre for Diffraction Data) database. Semiquantitative analyses were performed using MAUD software based on the Rietveld calculations.

Capillary water uptake tests were performed according to the European Standard UNI EN 15801:2010.[111] Before the investigation, the samples (prisms of 2.0×2.0×8.0 cm) were dried for 24h at 60 °C. The water absorption curve is expressed as Q (Kg m^{-2}) for the y-axis vs the square root of the absorption time (h$^{1/2}$) for the x axis. The slope of the curve in the initial steep region is the capillary absorption coefficient CA, calculated as:

$$CA = \frac{Q_i - Q_0}{t_1^{-1/2}}$$

Drying experiments were conducted according to NorMaL 29/88.[112] Soaked samples (marble and biomicrite prisms of 2.0×2.0×8.0 cm) were weighed at increasing time intervals. Drying curves were built, relating in abscissae the time in hours and in ordinate the water content wt in percentage. The drying index (DI), defined as the definite integral of the drying curve from the beginning (t_i) to end time (t_f) of the test, was then calculated by the following equation:

$$DI = \frac{\int_{t_i}^{t_f} f(wt)dt}{wt_{max} \cdot t_f}$$

where wt_{max} is the maximum water content at initial testing time.[113]

Vacuum water absorption tests were performed on all samples (marble and biomicrite prisms of 2.0×2.0×8.0 cm) according to UNE EN 1936:2010,[114] by maintaining the pressure at 0.2 kPa. From this free-water saturation method through Archimede's principle and buoyancy techniques the open porosity (P_o) of the stone samples can also be determined by:[115]

$$P_o = \frac{m_s - m_d}{m_s - m_h} \cdot 100$$

were m_d, m_h, and m_s are the mass values of the dry and saturated specimen in water and air, respectively. From these measurements, the real (ρ_r) and apparent density (ρ_{app}) were determined.[116] Pull-off tests were performed according to standard UNI EN 1015-12:2000 and used to evaluate the resistance to tearing of the sample.[117] Steel stubs, 20 mm in diameter, were grit blasted and attached to samples (marble cubes of 2.0×2.0×2.0 cm and biomicrite cubes of 3.0×3.0×3.0 cm) with an epoxy adhesive to form a butt joint. After the curing of the adhesive, the joints were then pulled in a universal testing machine fitted with a 5 kN load cell and tested at a rate of 2 mm/min at 25 °C. Strength values were then determined.

2.4 Theoretical calculations

Theoretical calculations were carried out at the density functional theory (DFT)[118] level with the Gaussian 16 commercial suite of programs (rev. B.01).[119] The PBE0 hybrid functional[120] was adopted, along with Ahlrichs

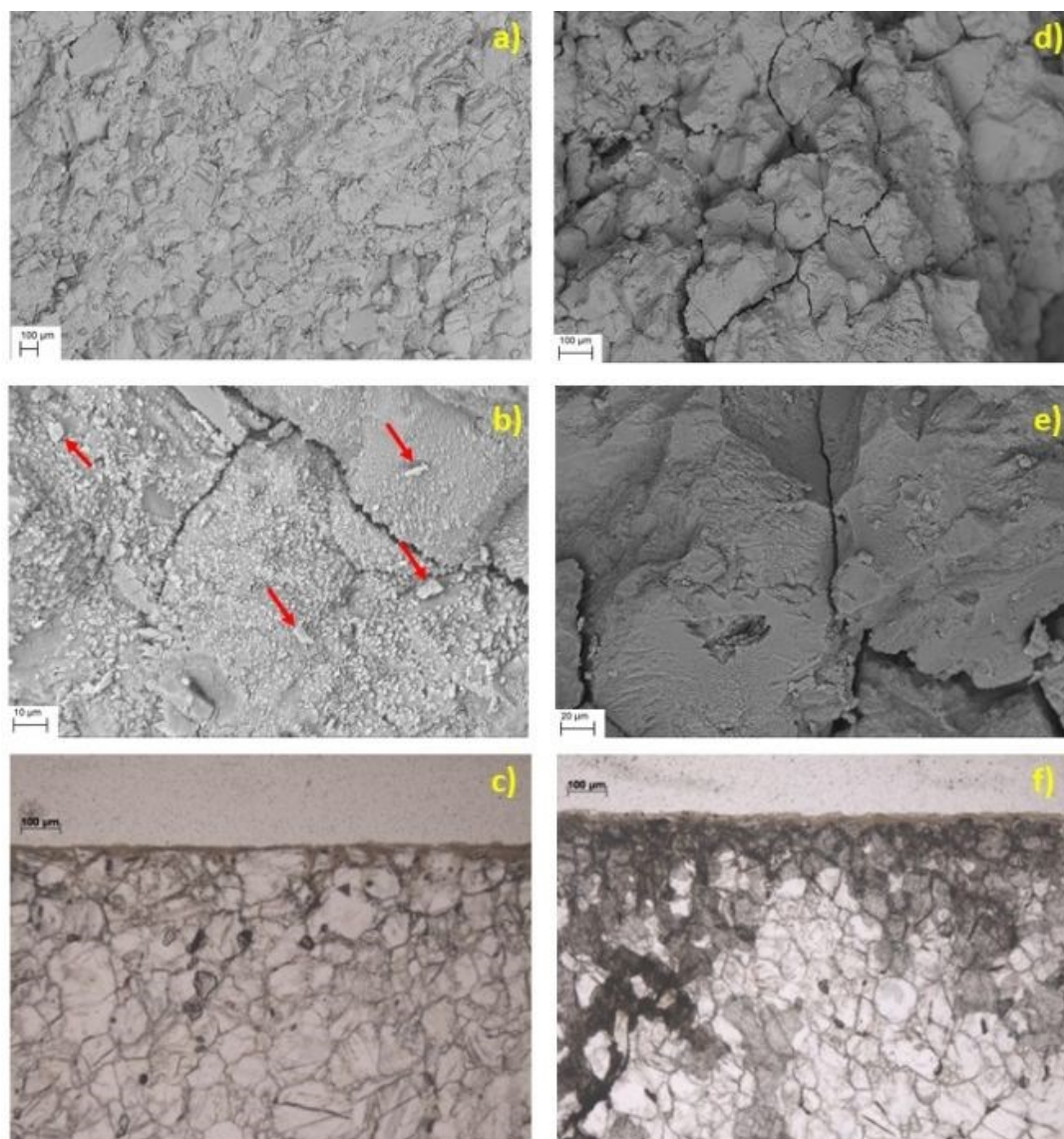**ARTICLE**   **Journal Name**

Fig. 1 SEM backscattered images of thermally weathered Carrara marble samples after the treatment with AmEtOx 5% (a–c) and 12% w/w (d–f) in water in static batch at room temperature for 24 h. Different magnifications are reported on the top (100 μm scale, a and d) and in the middle (10–20 μm scale, b and e), while sections of treated marble are shown on the bottom (c and f). The red arrows indicate larger crystals on the submicrometric crystalline coating.

triple-ζ basis sets (BSs) augmented with polarization functions, in the recent Weigend's formulation (def2-SVP).[121,122]

Solvation was implicitly taken into account by using the integral equation formalism of the polarizable continuous model (IEF-PCM) within the self-consistent reaction field (SCRF) approach.[123] Harmonic frequency calculations were carried out to verify the nature of the minima of each optimization by verifying the absence of significative negative frequencies. A potential energy surface (PES) study was carried out in order to evaluate the rotational barrier around the C–C bond of the

oxalate core. Natural charge distributions[124] were calculated at the optimized geometries at the same level of theory. The programs GaussView 6.0.16,[125] Molden 5.9,[126] and Chemissian 4.53[127] were used to investigate the optimized structures and molecular orbital shapes.

3. Results and discussion

3.1 Synthesis and characterization of AmEtOx

Ammonium monoethyloxalate, AmEtOx, was synthesized according to Scheme 1 and characterized by different microanalytic and spectroscopic techniques (see Experimental, Fig. S1 and Fig. S2 in ESI). UV-Vis spectroscopy measurements carried out at different concentrations (up to $2.0 \cdot 10^{-4}$ M) did not show any deviation from linearity. Spectrophotometric measurements showed that in saturated aqueous solution the solubility of this salt at 25 °C amounts to approximately 1.49 M (20.1% w/w, 201 g/L; K_{sp} = 2.22), i.e. it is more than 3 and 1.5 times more soluble than AmOx (0.4 M, 5% w/w, 50 g/L) and AmMeOx (1.01 M, 12.3% w/w, 140 g/L),[94] respectively.
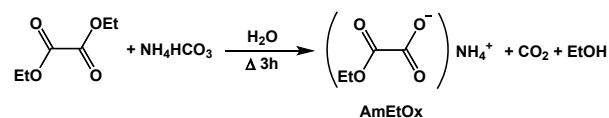
Scheme 1 Synthesis of AmEtOx

3.2 Effect of accelerated ageing on stone samples

Stone samples were subject to petrographic examinations (Fig. S3 in ESI). Optical microscopy observations in transmitted polarized light (TPL) on marble samples revealed that the crystalloblastic texture forms a mosaic or at times a non-oriented polygonal fabric, with grains generally ranging between 100 and 150 μm. The subhedral calcite crystals with well-defined straight boundaries often exhibited 120° junctions. Calcite accounts for over 99% of the substrate, with small accessory minerals of muscovite/illite and other phillosilicates. Opaque minerals were also observed.

Biomicritic limestone from Santa Caterina di Pittinuri, quarried from a Miocenic formation, is a lithotype common not only in Western Sardinia (Italy), but also in different countries overlooking the Mediterranean basin.[128] The biomicritic limestone exhibits poor physical-mechanical properties. Exfoliation, alveolation, erosion, pulverization, and crumbling are the most common weathering-induced decay forms. A very similar stone is the so-called "Globigerina Limestone" from the island of Malta.[129] The limestone, under petrographic microscope in cross-trasmitted polarized light (CTPL) mode, reveals an abundant microfossilifer fauna (50–60% of the total) embedded in a weakly carbonate cemented micrite matrix. Secondary components include a few very small (62–125 μm) grains of monocrystalline quartz (3.5%) and possibly iron oxyhydroxides or oxidized glauconite.

Notably, marble is more sensitive to thermal stresses than biomicrite, since the high porosity of biomicritic limestone allows to accommodate internal stresses and expansion of calcite micritic particles. In order to artificially reproduce the effects of natural thermal weathering in marble (granular disintegration), samples can be artificially decayed by means of a 600 °C thermal treatment.[16,106,130] The texture of artificially weathered marble reveals microcracks around the edges of specimens and detachment of boundary grains induced by the thermal differential expansion (Fig. S4b in ESI). Ultrasonic pulse velocity measurements are very useful for detecting stone defects and their evolution. Therefore, P-wave velocity (Vp) was measured before and after the thermal treatment. As expected, in the not-thermally-treated marble samples the Vp value was initially high ($5.7 \cdot 10^3$ km s^{-1}), but it steeply declined (by about 70%) after the thermal treatment, while the anisotropy index slightly increased (Table S2 in ESI). A second thermal treatment performed on marble weathered samples causes only minor effects on the microstructural, physical, and mechanical properties of the investigated samples. This is due to the fact that, after the first heating, micro-cracks developed in the sample, so that calcite crystal deformation can be partly accommodated in the newly-formed microcracks, resulting in reduced stress.[102] Mercury intrusion porosimetry (MIP) measurements showed that the porosity in the non-weathered samples was very low (0.5%), with an average pore diameter of 0.16 μm (Table 1). In thermally weathered samples, the total porosity grew to 6.9%, while the average pore size radius increased to

ARTICLE   Journal Name

Table 1 Mercury intrusion-determined porosity P (%), average pore diameter r_{av} (μm), modal pore diameter r_{md} (μm) determined for artificially weathered Carrara marble and biomicritic limestone before (untreated) and after treatment with AmEtOx aqueous solutions. Standard deviations are reported in parentheses.

	P	ΔP	r_{av}	Δr_{av} (%)	r_{md}	Δr_{md} (%)
Carrara white marble						
Untreated	6.9(7)	–	0.35(10)	–	1.80(5)	–
AmEtOx 5%	5.3(7)	−23	0.23(9)	−34	1.6(6)	−11
AmEtOx 12%	6.1(9)	−12	0.25(10)	−29	1.5(7)	−17
Biomicritic limestone						
Untreated	36.4[a]	–	0.42[a]	–	2.30[a]	–
AmEtOx 5%	34.3[a]	−6	0.27[a]	−36	1.50[a]	−35
AmEtOx 12%	32.3[a]	−11	0.29[a]	−31	1.47[a]	−36

[a] Standard deviation not reported due to the heterogeneity of the biomicrite samples.

0.35 μm. As a consequence, a small decrease in the apparent density of the samples after the thermal ageing was also observed (Table S2 in ESI). The combined results of Vp and MIP measurements describe a microstructure that closely resembles that exhibited by naturally weathered marbles,[20] thus confirming the suitability of the adopted artificial weathering method.

3.3 Effect of the treatment with AmEtOx on Carrara marble

Stone samples, similar in weight and in water open porosity, were treated with AmEtOx aqueous solutions according to the procedure previously adopted for AmMeox, AmOxam, and AmPhOxam.[94,95] Therefore, for the sake of comparison, the effects of the AmEtOx treatments were investigated at different w/w concentrations, namely 5% and 12% w/w. SEM images (Fig. 1) of the samples treated with the 12% w/w solution showed a newly-formed phase made of submicrometric crystals partially covering the surface of the stone, with calcite patches still visible. On the other hand, in samples treated with the 5% w/w solution, newly-formed crystals have been observed, belonging to two different size classes, a smaller one of submicrometric size and a larger one with few mm dimensions (red arrows in Fig. 1b). The coating provided by these crystals resulted more

homogeneous than in the case of the 12% w/w treatment. A better filling of the thermally generated micro-cracks can thus be observed. Thermally weathered marble samples treated with AmEtOx solutions exhibit a significant decrease in the MIP-determined porosity, amounting to 23% and 12% for 5% and 12% w/w AmEtOx solutions, respectively. The porosimetric distribution shows that a major fraction of macropores appears in the marble treated with the 12% AmEtOx aqueous solution as compared to the treatment with the diluted (5%) solution. This can be explained by taking into account that the coating formed at the surface, in the case of 12%, can be less coherent and homogeneous even if lightly thicker. These characteristics can be outlined also with microscopic observations. Parallelly to the variations in the porosity, the average pore size radius values were decreased by about 34% and 29%, respectively (Table 1). Both the average and modal pore diameter show a significant decrease indicating a shift in the dimensional distribution of the pores towards a smaller size (Table 1). In fact, the treatment with AmEtOx leads to a new pore size distribution, inducing a partial closure of the discontinuities in the range between 10 and 4 μm (Fig. S5 in ESI). X-Ray powder diffraction analyses on powdered treated samples revealed weddellite and whewellite along with the calcite signals (Fig. 2 and Fig. S6 in ESI), while no peaks ascribable to calcium monoethyloxalate were observed.

Journal Name

ARTICLE
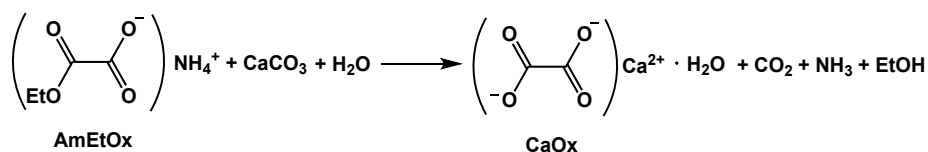
Scheme 2 Reaction of AmEtOx with $CaCO_3$ to give $CaOx \cdot H_2O$ (whewellite).

As mentioned above, in analogy to what it was observed for AmMeOx, this indicates a quantitative hydrolysis of AmEtOx,[94] resulting in the eventual formation of CaOx in its hydrated forms (Scheme 2 for whewellite). The SEM and XRD investigations thus confirm the formation of a layer of CaOx replacing calcite on the surface of the treated samples, whose lower solubility and higher stability under acidic conditions compared to calcium carbonate confers the coating passivating properties, protecting the stone from dissolution by rain.
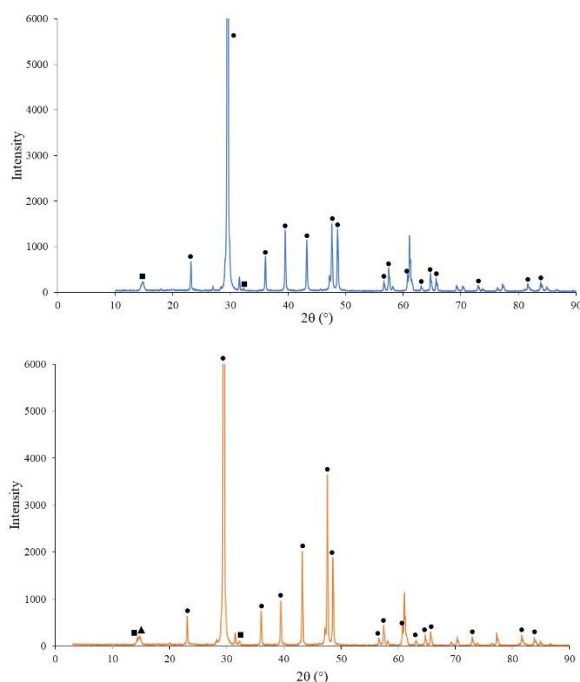

Fig. 2 X-Ray powder diffractograms of powdered thermally weathered Carrara marble samples treated with AmEtOx 5% (top) and 12% (bottom) w/w in water. Key symbols: ● Calcite; ▲ Whewellite; ■ Wheddellite.

In order to further confirm the presence of CaOx and to perform a cross-section analysis aimed at establishing the penetration depth of the treatments, a series of tts-μXRD measurements[131] were carried out on untreated and treated Carrara marble samples. First of all, 7 tts-μXRD measurements were carried out on the untreated marble samples at penetration depths between 0 and 360 μm. As expected, no peaks ascribable to CaOx, either in its monohydrate or dihydrate forms, were detected in the 3.9–4.1° 2θ interval. Subsequently, a sample treated with AmEtOx 5% w/w was analyzed through 13 measurement points sampled along a line (Fig. S7 in ESI), showing the presence of an approximately 30–50 μm thick layer of weddellite on the marble surface. In particular, the point centred at 10 μm is overwhelmingly $CaOx \cdot 2H_2O$, with only a small amount of calcite. A small amount of whewellite is also observed at approximately 45 μm depth. The XRD signal of calcium oxalates ends at ≈130 μm (Fig. S8 in ESI). On the other hand, in thin sections of samples treated with AmEtOx 12% w/w, three different zones can be recognized (Fig. S7 in ESI): i) a milky outer weddellite layer of ≤ 50 μm thickness (points 1 and 2); ii) large isometric calcite crystals (point 4); iii) sub-micrometric calcite including some weddellite crystals, as far as ≈200 μm from the surface (point 3). Therefore, the thickness of the passivating layer and the penetration depth of calcium oxalate resulting from the treatment with AmEtOx are larger than those of the homologue AmMeOx[94] and other previously tested compounds, such as AmPhOxam (Table S1 in ESI).[95] On considering the expected variability of the samples, the combined results of MIP, SEM and tts-μXRD measurements point to a comparable penetration depth (0.13–0.20 mm), although with a more homogeneous coating achieved by the treatment with AmEtOx 5% aqueous solution as compared with that carried out with the 12% w/w

ARTICLE   **Journal Name**

Table 2 Colorimetric measurements (average values of lightness $L*$, chromaticity coordinates $a*$ and $b*$, and colour differences ΔE^{CIE76} and $\Delta E^{CIE2000}$) determined for thermally weathered Carrara marble and biomicritic limestone before and after treatment with AmEtOx. Standard deviations are reported in parentheses.

	$L*$	$a*$	$b*$	ΔE^{CIE76}	$\Delta E^{CIE2000}$
Carrara white marble					
Untreated	92.4(2)	−0.15(1)	−0.27(2)	–	–
AmEtOx 5%	90.8(15)	−0.17(4)	1.94(16)	2.73	2.35
AmEtOx 12%	90.79(4)	−0.34(3)	2.08(1)	2.86	2.48
Biomicritic limestone					
Untreated	85.3(4)	1.83(3)	17.30(11)	–	–
AmEtOx 5%	84.0(2)	2.19(9)	15.7(6)	2.06	1.52
AmEtOx 12%	84.8(1)	1.84(2)	16.80(4)	0.68	0.43

Table 3 Capillary absorption coefficient CA (kg m^{-2} h$^{-1/2}$), drying index DI (% h^{-1}), open porosity P_o (%), relative ρ_r and apparent density ρ_{app} (g cm^{-3}) determined by water transport tests for thermally weathered Carrara marble and biomicritic limestone before and after treatment with AmEtOx. Standard deviations are reported in parentheses.

	CA	ΔCA	DI	ΔDI	P_o	ΔP_o	ρ_r	$\Delta\rho_r$	ρ_{app}	$\Delta\rho_{app}$
Carrara white marble										
Untreated	3.48		21.98		5.3(4)		2.7(0.2)		2.6(0.2)	
AmEtOx 5%	2.74	−21.3%	21.96	−0.1%	4.8(4)	−9.4%	2.6 (0.1)	−3.7%	2.5(0.2)	−3.8%
Biomicritic limestone										
Untreated	17.87		3.34		40.6(3)		2.8(0.2)		1.7(0.1)	
AmEtOx 5%	10.88	−39.1	2.88	−15.8%	38.7(3)	−4.7%	2.6(0.1)	−7.1%	1.6(0.1)	−5.8%

solution, thus suggesting that the concentration of the applied solution is not the only factor affecting the effectiveness of the treatment, and that other variables (such as the crystallization rate of the consolidant under different conditions) must also be considered. Colorimetric measurements performed on untreated and treated samples (Table 2) show only slight changes, with colour differences ΔE below the human eye detection limit (ΔE = 3).[48,132,133] The hydric behaviour of treated and untreated samples was also studied by means of different techniques, including water absorption by capillarity and drying tests (Fig. S9 in ESI), in order to ascertain the effects induced by the AmEtOx treatments on their water-transport properties. The treatment with the AmEtOx solution results in a small reduction in the water sorptivity (as testified by the Capillary absorption coefficient CA) and open porosity of the samples (Table 3), accompanied by a small but systematic decrease in the apparent density ρ_{app} as a consequence of the lower density of CaOx (2.29 and 2.02 g cm^{-3} for whewellite and weddellite, respectively) as compared to calcite (2.71 g cm^{-3}).[134] The cohesion of untreated and treated Carrara marble samples was evaluated through pull-off tests, which represent a practical method for estimating the direct tensile strength of rocks. An average maximum pull-off strength of 0.52(2) N·mm^{-2} was observed in the untreated weathered samples, and after the treatment an increase in the strength values up to 0.750(3) N·mm^{-2} was determined, thus indicating

Journal Name

ARTICLE
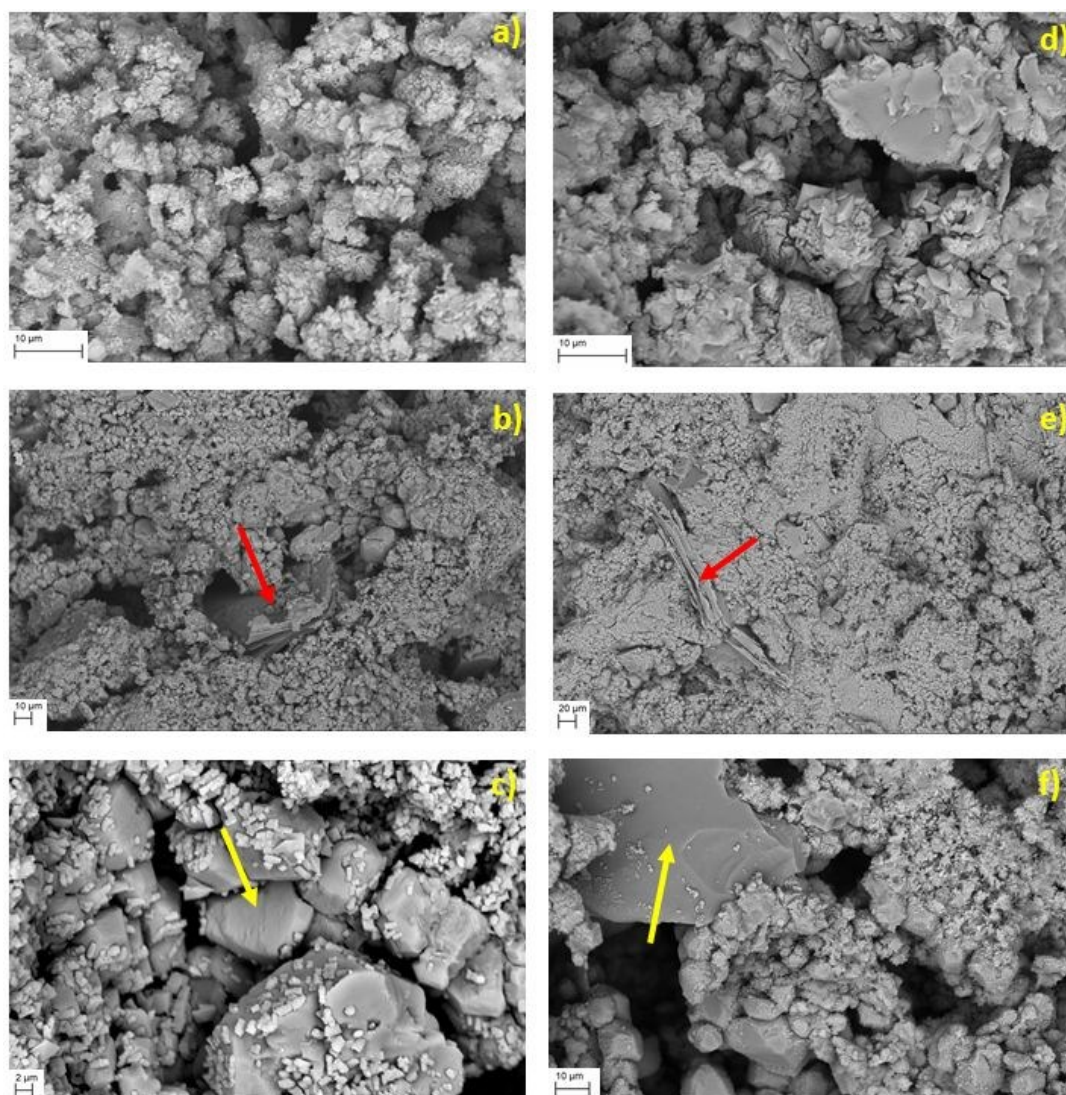
Fig. 3 SEM backscattered images of biomicritic limestone samples after the treatment with AmEtOx 5% (a–c) and 12% w/w (d–f) in water in static batch at room temperature for 24 h. The red and yellow arrows indicate the uncovered quartz and phyllosilicate crystals, respectively**.**
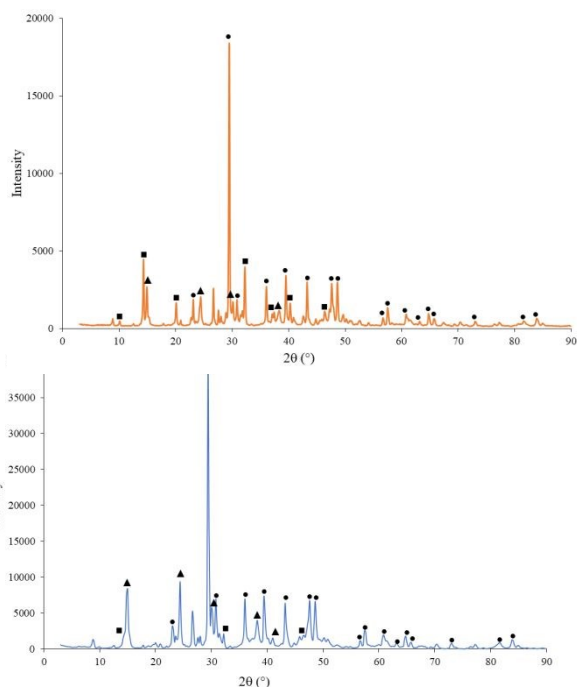
ARTICLE

an improved cohesion and strength of the lithic/stone material.

3.4 Effect of the treatment with AmEtOx on biomicritic limestone

Biomicritic limestone samples showed a decrease in the MIP-determined porosity when treated with 5% and 12% w/w solutions of AmEtOx (by about 6% and 11%, respectively, Table 1), while the average pore size radius values showed a more sensible variation, suggesting a pore size reduction particularly in the range 2–5 µm. A fraction of macropores in the range 50–300 µm also appeared after the treatment, slightly more evident in the case of the treatment with the 12% w/w solution (Fig. S10 in ESI). Therefore, the pore size distribution is the result of two effects due to the formation of the new CaOx coating: i) the refinement of the microstructure highlighted by a sharp increase of Hg intrusion starting from about 2 µm of pore radius distribution, and ii) the onset of a major fraction of


Fig. 4 X-Ray powder diffractograms of powdered biomicritic limestone samples treated with AmEtOx 5% (top) and 12% (bottom) w/w in water. Key symbols: ● Calcite; ▲ Whewellite; ■ Wheddellite.

macropores. These data suggest that the 12% w/w AmEtOx treatment reduces the intergranular porosity but simultaneously the fabric of the neogenic coating, although thicker, appears less coherent as compared to that formed by the more diluted AmEtOx solution, as microscopic observations have confirmed.

SEM images (Fig. 3) of the samples treated with both the 5% and the 12% w/w solution showed the formation of a homogeneous coating on the overall surface of limestone, consisting of the agglomeration of small crystals of submicrometric size. Uncovered spots corresponding to the quartz and muscovite crystals, not susceptible to surface attack by water even under acid conditions, are clearly visible in the SEM images, thus confirming the ability of oxalate derivatives to react selectively with calcite. X-Ray powder diffraction analyses on powdered treated samples confirmed also in this case that the coating formed after treatment with AmEtOx consists of calcium oxalate. In particular, after the treatment with AmEtOx 5% and 12% w/w, the peaks of both whewellite and weddellite were observed in addition to those of calcite, along with the signals of muscovite and quartz (Fig. 4 and Fig. S11 in ESI). A series of 12 aligned tts-µXRD measurements performed on an untreated biomicrite sample at penetration depths between 0 and 580 µm showed no diffraction peaks attributable to calcium oxalate phases in the 3.9-4.1° 2θ interval. Two lines (a and b) with 12 and 16 sampling points were measured on a thin section of a sample treated with the AmEtOx 5% w/w solution (Fig. S12, line a, in ESI), showing in both cases the presence of an approximately 200 µm thick layer of CaOx on the stone surface (Fig. S13 in ESI). The outermost layer of the coating is mostly made up of whewellite, while weddellite XRD signals appear at a depth of about 100 µm. The XRD signal of calcium oxalates is still present at ~500 µm for one of the lines. The samples treated with the AmEtOx 12% w/w solution were also sampled along two lines (a and b). Fig. S12 in SI shows the b sampling line and the CaOx coating (brighter) reaching a thickness of about 500 µm. The CaOx phases are detected as far as ~800 µm from the surface (Fig. S14 in ESI). Also in this case, the recorded penetration depths and thickness of the CaOx coating are larger than those previously estimated of AmOx,[65] AmMeOx, AmOxam,[94] and AmPhOxam (Table S1 in ESI).[95] Colourimetric measurements (Table 2) showed also in the case of biomicrite very small changes after treatment with AmEtOx (colour difference ∆E < 2), indicating that it does not induce significant chromatic variation of the stone. The studies carried out on the water transport properties of biomicritic samples (Fig. S15 in ESI) showed only a moderate decrease (about 5%) in the porosity accessible to water (Table 3), thus indicating that the shift of the size distribution towards smaller pores observed through MIP measurements does not significantly affect the hygric properties of the stone. Finally, pull-off tests indicated also in this case an improvement in the mechanic properties of the stone after treatment with AmEtOx, the average maximum pull-off strength passing from 1.10(1) N·mm⁻² to 2.46(0.2) N·mm⁻².

3.5 DFT calculations

With the aim of elucidating the reactivity of AmEtOx and its tendency to hydrolysis, Density Functional Theory (DFT)[118,135] calculations were performed on the monoethyloxalate anion EtOx⁻. Following the results of preliminary calculations previously performed in order to identify the most appropriate computational setup, [96] the PBE0[120] functional was adopted, in combination with the def2-TZVP triple-z basis sets (BSs)[121,122] equipped with polarization functions. The geometry of EtOx⁻ was optimized both in the gas phase and in water (modelled by using the IEF-PCM model of the SCRF theory),[123] and the nature of each structure was verified by a vibrational analysis.
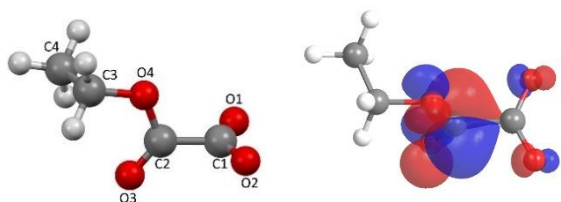
Fig. 5 Molecular drawing and atom labelling scheme for the EtOx⁻ anion at the optimized geometry in the gas phase (left) and isosurface of Kohn–Sham LUMO calculated at the optimized geometry in water (IEF-PCM SCRF model). Cutoff value = 0.05 |e|.

Only minor differences were found between the metric parameters optimized in the gas phase and in water, the main bond distances and angles differing by less than 0.03 Å and 4°, respectively (Table S3 in ESI). The geometry optimized in the gas phase shows a C1–C2 bond length of 1.542 Å and average C–O distances in the carboxylate group of 1.240 Å (Fig. 5 and Table S3 in ESI). These values were found to be in good agreement with the corresponding average structural data of the only crystal structure deposited in the CCDC featuring the EtOx⁻ anion (1.540 and 1.251 Å, respectively).[136] The almost identical length of the optimized C1–O1 and C1–O2 distances suggests a delocalized nature of the carboxylate group, which is expected for such systems. A very slight shortening of the C–C bond and a likewise lengthening of the C–O bonds was observed for the geometry optimized in water. Notwithstanding the only available structural data shows the anion in a planar conformation,[136] a dihedral angle O1–C1–C2–O4 (twist angle t) of 88.19 and 84.56° was found in the gas phase and in water, respectively, when the metric parameters of EtOx⁻ were optimized without any geometrical constrains. In fact, in the previously reported investigation[96] a general tendency to assume this staggered conformation (torsion angle τ = 90.0°, D_{2d} point group) was observed for the $C_2O_4^{2-}$ oxalate anion (Ox²⁻) and its monomethyl- and monophenyl-substituted esters (MeOx⁻ and PhOx⁻, respectively), while an opposite behavior was shown by oxamate, methyloxamate, and phenyloxamate, which were calculated to favor the planar conformation (τ = 0.0°, D_{2h} point group). In order to verify the possibility for the EtOx⁻ anion to assume a staggered conformation, the rotational barrier of the torsion angle τ was calculated in the gas phase, by carrying out a potential energy scan (PES) as a function of τ (Fig.

S16 in ESI). The staggered conformation (τ = 90.0°, D_{2d}) was calculated to be more stable than the planar one (τ = 0.0°, D_{2h}) by only 2.84 kcal mol⁻¹, thus confirming a small rotational barrier around the C1–C2 bond. An examination of the virtual molecular orbitals calculated in water for EtOx⁻ in its staggered conformation shows the presence of a Kohn–Sham LUMO (Lowest Unoccupied Molecular Orbital) mostly localized on the C2 atom (Fig. 5). On the other hand, a natural charge of 0.673 |e| was calculated on the atom C2 in water. The positive charge on carbon atom of the ester function, along with the composition of the LUMO, accounts for the tendency to hydrolysis observed experimentally for AmEtOx in water solution, in agreement with the calculated data previously reported for the methyl analogue in the gas phase.[96] The combination of experimental data and DFT calculations thus confirms that the application of aqueous solutions of monoester derivatives of oxalic acid ROx⁻ invariably leads to its hydrolysis accompanied by the conversion of superficial calcium carbonate into calcium oxalate CaOx, rather than the expected calcium salts CaROx (R = Me, Et).

4. Conclusions

The salt AmEtOx was synthesized, characterized, and tested, in two different concentrations (5% and 12% w/w), as a conservation agent on Carrara marble and biomicritic limestone. AmEtOx readily reacts with calcite to give ammonium oxalate mono- or dihydrate, and thus represents an alternative, more soluble precursor to CaOx than AmOx, with a better penetration and filler capability. AmEtOx overcomes the limits of the previously reported AmMeOx salt, being remarkably more water soluble (C = 1.49 and 1.01 M for AmEtOx and AmMeOx, respectively) and providing a larger depth of penetration within both Carrara marble and biomicritic limestone, thus guaranteeing a more effective CaOx deposition. In fact, SEM images and tts-µXRD measurements confirm that after the treatment with AmEtOx, Carrara marble and biomicritic limestones were covered by a newly-formed 30–50 and 200–500 µm thick crystalline coating of whewellite and weddellite, respectively, with CaOx phases detectable up to ~800 µm from the surface in the case of biomicrite: notably, in the case of AmOx and our previously synthesized derivatives (AmMeOx AmOxAm, and AmPhOxam) protective layers few µm or up to just few tens µm thick were determined (Table S1 in ESI). Variations in the uniformity of the coating depending on the used concentration of AmEtOx were observed. In all cases, a small reduction in the porosity of the stone sample was observed after treatment with AmEtOx, which resulted particularly significative for the Carrara marble, and was accompanied by a slight decrease in the average pore size. As known, material durability could be compromised by a strong reduction in pore size respect to salt attack with increase of crystallization pressure. On the other hand, we observed only a refinement of the porous structure with a small shift toward smaller pores. The presence of a coating along with such reduction in pore size could inhibit the vehiculation of hazardous material inside the stone. Moreover, the treatment

with AmEtOx on both Carrara marble and biomicritic samples resulted in an enhancement in their cohesion (as indicated by pull-off tests), resulting in an increase in the intrinsic strength of the material towards such hazards and – more in general – towards decay. This strengthening is accompanied by no perceptible alterations in colour or vapor permeability, thus testifying the compatibility of the treatment with the stone substrates. Finally, DFT calculations gave insights into the electronic properties leading to the tendency of hydrolysis shown by AmEtOx and its analogue AmMeOx, and the inferred structure-properties relationships may be used to guide the future design of related agents. This investigation confirms that the salts of monoester derivatives of oxalic acid represent a promising class of new materials for the conservation of carbonate stones or other artificial materials, such as ancient lime-based mortars, against dissolution by rain. The tendency of hydrolysis in aqueous solution allows to obtain a passivating coating on the stone starting from water solutions featuring molar concentrations of about 1.5 M, up to more than three times that achievable with the parent ammonium oxalate solution (0.4 M). The improvement of the coating features (e.g. adhesion, thickness, cohesion, and covering effectiveness) will guide future studies on the experimentation of different application techniques for this class of compounds, also with the employment of nanoparticles and biomineralization techniques, as well as the long-term effectiveness and conservation abilities of the treatments will also be studied.

Conflicts of interest

There are no conflicts to declare.

Acknowledgements

References

1   D. Eric and C. A. Price, in *Stone in architecture. 2nd ed. Los Angeles (CA): America Library of Congress Cataloging-in-Publication Data*, 2010, pp. 1–176.

2   A. E. Charola and R. Ware, *Geol. Soc. Spec. Publ.*, 2002, **205**, 393–406.

3   E. Hansen, E. Doehne, J. Fidler, J. Larson, B. Martin, M. Matteini, C. Rodriguez-Navarro, E. S. Pardo, C. Price, A. de Tagle, J. M. Teutonico and N. Weiss, *Stud. Conserv.*, 2003, **48**, 13–25.

4   *Limestones in the Built Environment: Present-day challenges for the preservation of the past, B.J.Smith, M. Gomez-Heras, H.A.Viles and J.Cassar eds. Geological Society, Special Publication 331, London, 2010.*, Wiley, 2014, vol. 49.

5   M. Steiger, A. E. Charola and K. Sterflinger, in *Stone in Architecture: Properties, Durability*, Springer Berlin Heidelberg, 2011, pp. 227–316.

6   A. P. Ferreira Pinto and J. Delgado Rodrigues, *J. Cult. Herit.*, 2012, **13**, 154–166.

7   M. E. Weaver, G. G. Amoroso and V. Fassina, *Stone Decay and Conservation: Atmospheric Pollution, Cleaning, Consolidation and Protecting*, JSTOR, 1985, vol. 17.

8   S. Columbu, S. Carboni, S. Pagnotta, M. Lezzerini, S. Raneri, S. Legnaioli, V. Palleschi and A. Usai, *Spectrochim. Acta Part B At. Spectrosc.*, 2018, **149**, 62–70.

9   G. Toreno, D. Isola, P. Meloni, G. Carcangiu, L. Selbmann, S. Onofri, G. Caneva and L. Zucconi, *J. Cult. Herit.*, 2018, **30**, 100–109.

10   L. N. Plummer and E. Busenberg, *Geochim. Cosmochim. Acta*, 1982, **46**, 1011–1040.

11   S. Naidu, J. Blair and G. W. Scherer, *J. Am. Ceram. Soc.*, 2016, **99**, 3421–3428.

12   P. V. Brady, *Choice Rev. Online*, 1997, **34**, 34-3876-34–3876.

13   A. P. F. Pinto and J. D. Rodrigues, *J. Cult. Herit.*, 2008, **9**, 38–53.

14   S. Columbu, C. Lisci, F. Sitzia and G. Buccellato, *Environ. earth Sci.*, 2017, **76**, 148.

15   G. Graziani, E. Sassoni, G. W. Scherer and E. Franzoni, *Corros. Sci.*, 2017, **127**, 168–174.

16   E. Franzoni, E. Sassoni, G. W. Scherer and S. Naidu, *J. Cult. Herit.*, 2013, **14**, e85–e93.

17   E. Franzoni and E. Sassoni, *Sci. Total Environ.*, 2011, **412–413**, 278–285.

18   E. Sassoni, G. Graziani and E. Franzoni, *Mater. Des.*, 2015, **88**, 1145–1157.

19   J. Martínez-Martínez, D. Benavente, M. Gomez-Heras, L. Marco-Castaño and M. Á. García-Del-Cura, *Constr. Build. Mater.*, 2013, **38**, 443–454.

20   S. Siegesmund, K. Ullemeyer, T. Weiss and E. K. Tschegg, *Int. J. Earth Sci.*, 2000, **89**, 170–182.

21   E. Sassoni, G. Graziani, G. Ridolfi, M. C. Bignozzi and E. Franzoni, *Mater. Des.*, 2017, **120**, 345–353.

22   C. Pesce, L. M. Moretto, E. F. Orsega, G. L. Pesce, M. Corradi and J. Weber, *Materials (Basel).*, 2019, **12**, 3025.

23   S. Columbu, F. Sitzia and G. Ennas, *Archaeol. Anthropol. Sci.*, 2017, **9**, 523–553.

24   M. Lezzerini, S. Raneri, S. Pagnotta, S. Columbu and G. Gallello, *Measurement*, 2018, **126**, 322–331.

25   E. Sassoni, G. Graziani and E. Franzoni, *Constr. Build. Mater.*, 2016, **102**, 918–930.

26   G. Torraca, *Porous Building Materials, 3rd ed.*, International Centre for theStudy of the Preservation and Restoration of Cultural Property, Rome, Italy, 1988.

27   B. Sena da Fonseca, A. P. Ferreira Pinto, S. Piçarra and M. F. Montemor, *Constr. Build. Mater.*, 2018, **163**, 586–599.

28   X. Ma, M. Balonis, H. Pasco, M. Toumazou, D. Counts and I. Kakoulli, *Constr. Build. Mater.*, 2017, **150**, 333–344.

29   M. Ambrosi, L. Dei, R. Giorgi, C. Neto and P. Baglioni, *Langmuir*, 2001, **17**, 4251–4255.

30   M. L. Weththimuni, M. Licchelli, M. Malagodi, N. Rovella and M. La Russa, *Meas. J. Int. Meas. Confed.*, 2018, **127**, 396–405.

31   T. Skoulikidis, P. Vassiliou and K. Tsakona, *Environ. Sci. Pollut. Res.*, 2005, **12**, 28–33.

32   P. Baglioni, D. Chelazzi, R. Giorgi, E. Carretti, N. Toccafondi and Y. Jaidar, *Appl. Phys. A Mater. Sci. Process.*, 2014, **114**, 723–732.

33   J. Otero, V. Starinieri and A. E. Charola, *Constr. Build. Mater.*, 2018, **181**, 394–407.

34   E. Carretti and L. Dei, *Prog. Org. Coatings*, 2004, **49**, 282–289.

35   O. Chiantore and M. Lazzari, *Polymer (Guildf).*, 2001, **42**, 17–27.

36   M. Favaro, R. Mendichi, F. Ossola, U. Russo, S. Simon, P. Tomasin and P. A. Vigato, *Polym. Degrad. Stab.*, 2006, **91**, 3083–3096.

37   Y. Cao, A. Salvini and M. Camaiti, *J. Cult. Herit.*, 2020, **44**, 90–97.

38   Y. Cao, A. Salvini and M. Camaiti, *Prog. Org. Coatings*, 2017, **111**, 164–174.

39   M. Mazzola, P. Frediani, S. Bracci and A. Salvini, *Eur. Polym. J.*, 2003, **39**, 1995–2003.

40   P. Baglioni and R. Giorgi, *Soft Matter*, 2006, 2, 293–303.

41   M. Matteini, *Conserv. Sci. Cult. Herit.*, 2008, **8**, 13–27.

42   G. Wheeler, *Alkoxysilanes and the Consolidation of Stone*, 2005, vol. 46.

43   G. W. Scherer and G. S. Wheeler, *Key Eng. Mater.*, 2009, **391**, 1–25.

44   G. Graziani, E. Sassoni, E. Franzoni and G. W. Scherer, *Appl. Surf. Sci.*, 2016, **368**, 241–257.

45   E. Sassoni, S. Naidu and G. W. Scherer, *J. Cult. Herit.*, 2011, **12**, 346–355.

46   E. Sassoni, E. Franzoni, B. Pigino, G. W. Scherer and S. Naidu, *J. Cult. Herit.*, 2013, **14**, e103–e108.

47   E. Possenti, C. Colombo, D. Bersani, M. Bertasa, A. Botteon, C. Conti, P. P. Lottici and M. Realini, *Microchem. J.*, 2016, **127**, 79–86.

48   M. Matteini, S. Rescic, F. Fratini and G. Botticelli, *Int. J. Archit. Herit.*, 2011, **5**, 717–736.

49   S. Naidu and G. W. Scherer, *J. Colloid Interface Sci.*, 2014, **435**, 128–137.

50   E. Sassoni, *Materials (Basel).*, 2018, **11**, 557.

ARTICLE

51 D. Mudronja, F. Vanmeert, K. Hellemans, S. Fazinic, K. Janssens, D. Tibljas, M. Rogosic and S. Jakovljevic, *Appl. Phys. A Mater. Sci. Process.*, 2013, **111**, 109–119.

52 B. Doherty, M. Pamplona, C. Miliani, M. Matteini, A. Sgamellotti and B. Brunetti, *J. Cult. Herit.*, 2007, **8**, 186–192.

53 B. Salvadori, D. Pinna and S. Porcinai, *Environ. Sci. Pollut. Res.*, 2014, **21**, 1884–1896.

54 D. Pinna, B. Salvadori and S. Porcinai, *Constr. Build. Mater.*, 2011, **25**, 2723–2732.

55 A. Burgos-Cara, E. Ruiz-Agudo and C. Rodriguez-Navarro, *Mater. Des.*, 2017, **115**, 82–92.

56 B. Doherty, M. Pamplona, R. Selvaggi, C. Miliani, M. Matteini, A. Sgamellotti and B. Brunetti, *Appl. Surf. Sci.*, 2007, **253**, 4477–4484.

57 W. H. McComas and W. Rieman, *J. Am. Chem. Soc.*, 1942, **64**, 2946–2947.

58 L. Brečević, D. Škrtić and J. Garside, *J. Cryst. Growth*, 1986, **74**, 399–408.

59 N. V. Gvozdev, E. V. Petrova, T. G. Chernevich, O. A. Shustin and L. N. Rashkovich, *J. Cryst. Growth*, 2004, **261**, 539–548.

60 C. Conti, M. Casati, C. Colombo, M. Realini, L. Brambilla and G. Zerbi, *Spectrochim. Acta - Part A Mol. Biomol. Spectrosc.*, 2014, **128**, 413–419.

61 M. B. McBride, S. Kelch, M. Schmidt, Y. Zhou, L. Aristilde and C. E. Martinez, *Environ. Sci. Technol.*, 2019, **53**, 13794–13801.

62 M. Del Monte, C. Sabbioni and G. Zappia, *Sci. Total Environ.*, 1987, **67**, 17–39.

63 L. Rampazzi, *J. Cult. Herit.*, 2019, 40, 195–214.

64 A. E. Hill and E. F. Distler, *J. Am. Chem. Soc.*, 1935, **57**, 2203–2204.

65 T. M. Cezar, *J. Conserv. Museum Stud.*, 1998, **4**, 6–10.

66 A. E. Charola, S. A. Centeno and K. Normandin, *J. Archit. Conserv.*, 2010, **16**, 29–44.

67 C. Conti, C. Colombo, G. Festa, J. Hovind, E. P. Cippo, E. Possenti and M. Realini, *J. Cult. Herit.*, 2016, **19**, 463–466.

68 M. L. Tabasso and S. Simon, *Stud. Conserv.*, 2006, **51**, 67–82.

69 E. Sassoni, G. Graziani, E. Franzoni and G. W. Scherer, *Corros. Sci.*, 2018, **136**, 255–267.

70 B. Sena da Fonseca, M. J. Ferreira, M. G. Taryba, S. Piçarra, A. P. Ferreira Pinto and M. de F. Montemor, *J. Cult. Herit.*, 2019, **37**, 63–72.

71 E. Franzoni, E. Sassoni and G. Graziani, *J. Cult. Herit.*, 2015, **16**, 173–184.

72 A. Murru and R. Fort, *J. Cult. Herit.*, 2020, **42**, 45–55.

73 G. Graziani, E. Sassoni, G. W. Scherer and E. Franzoni, *Constr. Build. Mater.*, 2017, **148**, 571–578.

74 S. A. Ruffolo, M. F. La Russa, P. Aloise, C. M. Belfiore, A. Macchia, A. Pezzino and G. M. Crisci, *Appl. Phys. A Mater. Sci. Process.*, 2014, **114**, 753–758.

75 R. Giorgi, L. Dei and P. Baglioni, *Stud. Conserv.*, 2000, **45**, 154–161.

76 D. Chelazzi, G. Poggi, Y. Jaidar, N. Toccafondi, R. Giorgi and P. Baglioni, *J. Colloid Interface Sci.*, 2013, **392**, 42–49.

77 D. Chelazzi, R. Camerini, R. Giorgi and P. Baglioni, *Adv. Mater. Conserv. Stone*, 2018, 151–173.

78 L. De Ferri, P. P. Lottici, A. Lorenzi, A. Montenero and E. Salvioli-Mariani, *J. Cult. Herit.*, 2011, **12**, 356–363.

79 L. Dei and B. Salvadori, *J. Cult. Herit.*, 2006, **7**, 110–115.

80 J. Otero, A. E. Charola, C. A. Grissom and V. Starinieri, *Ge-Conservacion*, 2017, **1**, 71–78.

81 I. Natali, M. L. Saladino, F. Andriulo, D. Chillura Martino, E. Caponetti, E. Carretti and L. Dei, *J. Cult. Herit.*, 2014, **15**, 151–158.

82 M. I. Daskalakis, A. Magoulas, G. Kotoulas, I. Katsikis, A. Bakolas, A. P. Karageorgis, A. Mavridou, D. Doulia and F. Rigas, *Appl. Microbiol. Biotechnol.*, 2014, **98**, 6871–6883.

83   C. Rodriguez-Navarro, M. Rodriguez-Gallego, K. Ben Chekroun and M. T. Gonzalez-Muñoz, *Appl. Environ. Microbiol.*, 2003, **69**, 2182–2193.

84   T. Li, Y. Hu and B. Zhang, *Front. Microbiol.*, 2018, **9**, 3025.

85   J. Vincent, R. Sabot, I. Lanneluc, P. Refait, P. Turcry, P.-Y. Mahieux, M. Jeannin and S. Sablé, *Matériaux Tech.*, 2020, **108**, 302.

86   J. T. DeJong, M. B. Fritzges and K. Nüsslein, *J. Geotech. Geoenvironmental Eng.*, 2006, **132**, 1381–1392.

87   P. Tiano, L. Biagiotti and G. Mastromei, *J. Microbiol. Methods*, 1999, **36**, 139–145.

88   K. V. Sazanova (nee Barinova), O. V. Frank-Kamenetskaya, D. Y. Vlasov, M. S. Zelenskaya, A. D. Vlasov, A. V. Rusakov and M. A. Petrova, *Crystals*, 2020, **10**, 756.

89   K. Kolo and P. Claeys, *Biogeosciences Discuss.*, 2005, **2**, 451–497.

90   A. Webster and E. May, *Trends Biotechnol.*, 2006, 24, 255–260.

91   V. Achal and A. Mukherjee, *Constr. Build. Mater.*, 2015, 93, 1224–1235.

92   N. Kaur, M. S. Reddy and A. Mukherjee, *J. Microbiol. Biotechnol.*, 2013, **23**, 707–714.

93   E. Ortega-Villamagua, M. Gudiño-Gomezjurado and A. Palma-Cando, *Molecules*, 2020, **25**, 5499.

94   L. Maiore, M. C. Aragoni, G. Carcangiu, O. Cocco, F. Isaia, V. Lippolis, P. Meloni, A. Murru, E. Tuveri and M. Arca, *J. Colloid Interface Sci.*, 2015, **448**, 320–330.

95   L. Maiore, M. C. Aragoni, G. Carcangiu, O. Cocco, F. Isaia, V. Lippolis, P. Meloni, A. Murru, A. M. Z. Slawin, E. Tuveri, J. D. Woollins and M. Arca, *New J. Chem.*, 2016, **40**, 2768–2774.

96   A. Pintus, M. C. Aragoni, G. Carcangiu, L. Giacopetti, F. Isaia, V. Lippolis, L. Maiore, P. Meloni and M. Arca, *New J. Chem.*, 2018, **42**, 11593–11600.

97   C. Buosi, S. Columbu, G. Ennas, P. Pittau and G. G. Scanu, *Geoheritage*, 2019, **11**, 729–749.

98   S. Columbu, G. Cruciani, D. Fancello, M. Franceschelli and G. Musumeci, *Eur. J. Mineral.*, 2015, **27**, 471–486.

99   S. Columbu, F. Antonelli and F. Sitzia, *Mediterr. Archaeol. Archaeom.*, 2018, **18**, 37–64.

100   A. Moropoulou, K. Polikreti, A. Bakolas and P. Michailidis, *Cem. Concr. Res.*, 2003, **33**, 891–898.

101   *UNI 9724-4. Materiali lapidei. Confezionamento sezioni sottili e lucide*, Ente Nazionale Italiano di Unificazione, Milan, Italy, 1999.

102   E. Sassoni and E. Franzoni, *Appl. Phys. A Mater. Sci. Process.*, 2014, **115**, 809–816.

103   *EN 12407. Natural stone test methods - Petrographic examination*, Ente Nazionale Italiano di Unificazione, Milan, Italy, 2007.

104   J. Guyader and A. Denis, *Bull. Int. Assoc. Eng. Geol. - Bull. l'Association Int. Géologie l'Ingénieur*, 1986, **33**, 49–55.

105   R. Fort, M. J. Varas, M. Alvarez de Buergo and D. Martin-Freire, *J. Geophys. Eng.*, 2011, **8**, S132–S144.

106   A. Murru, D. M. Freire-Lista, R. Fort, M. J. Varas-Muriel and P. Meloni, *Constr. Build. Mater.*, 2018, **186**, 1200–1211.

107   J. Rius, O. Vallcorba, C. Frontera, I. Peral, A. Crespi and C. Miravitlles, *IUCrJ*, 2015, **2**, 452–463.

108   F. Fauth, I. Peral, C. Popescu and M. Knapp, *Powder Diffr.*, 2013, **28**, S360–S370.

109   O. Vallcorba and J. Rius, *J. Appl. Crystallogr.*, 2019, **52**, 478–484.

110   C. Kapridaki and P. Maravelaki-Kalaitzaki, *Prog. Org. Coatings*, 2013, **76**, 400–410.

111   *EN 15801. Conservation of cultural property - test methods - determination of water absorption by capillarity*, Ente Nazionale Italiano di Unificazione, Milan, Italy, 2010.

112   *NORMAL 29/88: Misura dell'indice di asciugamento (dryng index)*, CNR-ICR (Consiglio Nazionale delle Ricerche - Istituto Centrale per il Restauro), Rome, Italy, 1988.

113   J. Grilo, P. Faria, R. Veiga, A. Santos Silva, V. Silva and A.

Velosa, *Constr. Build. Mater.*, 2014, **54**, 378–384.

114 *EN 1936. Natural Stone Test Methods - Determination of Real Density and Apparent Density, and of Total and Open Porosity*, Turkish Standard Institute, Ankara, Turkey, 2007.

115 İ. Uğur and H. Ö. Toklu, *Bull. Eng. Geol. Environ.*, 2020, **79**, 255–267.

116 C. Hall and A. Hamilton, *Mater. Struct. Constr.*, 2016, **49**, 3969–3979.

117 *EN 1015-12. Methods of test for mortar for masonry–Part. 12: Determination of adhesive strength of hardened rendering and plastering mortars on substrates*, Ente Nazionale Italiano di Unificazione, Milan, Italy, 2000.

118 W. Koch and M. C. Holthausen, *A chemist's guide to density functional theory*, Wiley-VCH, 2001.

119 M. J. Frisch, G. W. Trucks, H. B. Schlegel, G. E. Scuseria, M. A. Robb, J. R. Cheeseman, G. Scalmani, V. A. Barone, P. G., H. Nakatsuji, X. Li, M. Caricato, A. V. Marenich, J. Bloino, B. G. Janesko, R. Gomperts, B. Mennucci, H. P. Hratchian, J. V. Ortiz, A. F. Izmaylov, J. L. Sonnenberg, D. Williams-Young, F. Ding, F. Lipparini, F. Egidi, J. Goings, B. Peng, A. Petrone, T. Henderson, D. Ranasinghe, V. G. Zakrzewski, J. Gao, N. Rega, G. Zheng, W. Liang, M. Hada, M. Ehara, K. Toyota, R. Fukuda, J. Hasegawa, M. Ishida, T. Nakajima, Y. Honda, O. Kitao, H. Nakai, T. Vreven, K. Throssell, J. Montgomery, J. A., J. E. Peralta, F. Ogliaro, M. Bearpark, J. J. Heyd, E. N. Brothers, K. N. Kudin, V. N. Staroverov, R. Kobayashi, J. Normand, K. Raghavachari, A. P. Rendell, B. J. C., S. S. Iyengar, J. Tomasi, M. Cossi, J. M. Millam, M. Klene, C. Adamo, R. Cammi, J. W. Ochterski, R. L. Martin, M. K., O. Farkas, J. B. Foresman and D. J. Fox, *Gaussian 16 Rev. B. 01, Wallingford, CT*, 2016.

120 C. Adamo and V. Barone, *J. Chem. Phys.*, 1999, **110**, 6158–6170.

121 F. Weigend and R. Ahlrichs, *Phys. Chem. Chem. Phys.*, 2005, **7**, 3297–3305.

122 F. Weigend, *Phys. Chem. Chem. Phys.*, 2006, **8**, 1057–1065.

123 J. Tomasi, B. Mennucci and R. Cammi, *Chem. Rev.*, 2005, 105, 2999–3093.

124 A. E. Reed, L. A. Curtiss and F. Weinhold, *Chem. Rev.*, 1988, **88**, 899–926.

125 R. Dennington, T. A. Keith and J. M. Millam, *GaussView version 6.0. 16*, Semichem Inc. Shawnee Mission KS, 2016.

126 G. Schaftenaar and J. H. Noordik, *J. Comput. Aided. Mol. Des.*, 2000, **14**, 123–134.

127 L. V Skripnikov, *Chemissian Version 4.53, Visualization Computer Program*, 2017.

128 A. Cherchi, *Mém. BRGM*, 1974, **78**, 433–445.

129 J. Cassar, *Geol. Soc. Spec. Publ.*, 2002, **205**, 33–49.

130 J. M. Logan, *Environ. Geol.*, 2004, **46**, 456–467.

131 L. Maritan, L. Casas, A. Crespi, E. Gravagna, J. Rius, O. Vallcorba and D. Usai, *Herit. Sci.*, 2018, **6**, 74.

132 W. S. Mokrzycki and M. Tatol, *Mach. Graph. Vis.*, 2011, **20**, 383–411.

133 J. D. Rodrigues and A. Grossi, *J. Cult. Herit.*, 2007, **8**, 32–43.

134 Mineralogy Database, http://webmineral.com/.

135 A. J. Cohen, P. Mori-Sánchez and W. Yang, *Chem. Rev.*, 2012, **112**, 289–320.

136 X. Deng, J. T. Liang, M. Peterson, R. Rynberg, E. Cheung and N. S. Mani, *J. Org. Chem.*, 2010, **75**, 1940–1947.